Computation of Reflected and Transmitted Horn Radiation Patterns for a Dichroic Plate

J. C. Chen
Ground Antennas and Facilities Engineering Section

A previous dichroic plate analysis has assumed that an ideal uniform plane wave illuminates the dichroic plate at a single angle of incidence. In fact, a horn radiates energy at the dichroic plate and illuminates it at many different angles. To model the horn and dichroic plate system, the horn pattern is represented as a group of plane waves traveling in different directions. The details of this analysis are presented in this article. The calculated and measured reflected radiation patterns show good agreement. The noise temperature predicted from the horn pattern model is shown to be more accurate than that from a simple plane-wave model.

I. Introduction

The dichroic plate under consideration is a metal plate perforated with identical apertures spaced on a periodic grid. The periodic characteristics of the dichroic plate simplify the analysis to the consideration of a single unit cell [1]. Computer codes have been developed to analyze the response of the dichroic plate assuming uniform plane-wave incidence (Fig. 1). In practice, energy radiated from a horn strikes the dichroic plate in many directions (Fig. 2). The transmission loss for energy incident at a nondesign angle is usually greater than that at the design angle. The horn pattern incidence analysis presented below will improve the understanding of dichroic plate performance for horn pattern incidence, allowing the computation of the transmitted and reflected patterns as well as the noise temperature contribution of the dichroic plate.

II. Analysis

The first step in modeling the horn and dichroic plate system is to consider the horn pattern as a group of plane waves traveling at different angles. Each plane wave has a certain amplitude and phase and strikes the plate at a different angle of incidence. The scattering matrix of the dichroic plate is calculated at the angle of incidence for each plane-wave component. Finally, the transmitted and reflected plane waves are summed up to form the transmitted and reflected radiation patterns.

The far-field horn pattern can be decomposed as a group of plane waves of different amplitudes and phases traveling at different directions. For example, the 26-dB Ka-band horn pattern at 32 GHz is considered to be a plane wave traveling at $\theta = 0$ deg and $\phi = 0$ deg, with an amplitude of 0 dB, plus a second plane wave traveling at $\theta = 1$ deg and $\phi = 0$ deg, with an amplitude of -0.137 dB, etc. (Fig. 3). Basically, the horn pattern is sampled as shown in Fig. 3. Each plane wave radiates from the horn in the

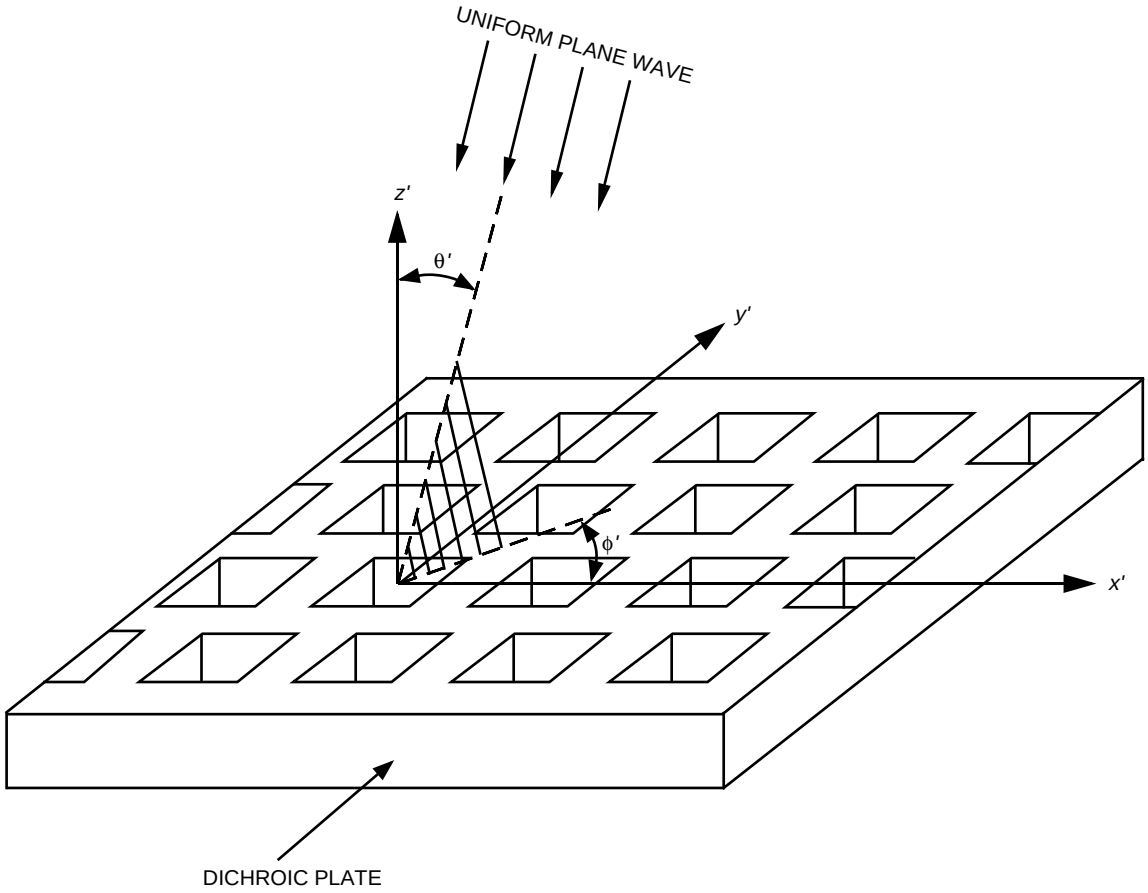

Fig. 1. The dichroic plate with uniform plane-wave incidence.

(θ, ϕ) direction with respect to the horn axis and strikes the dichroic plate at (θ', ϕ') with respect to the normal direction of the dichroic plate, as described in Appendix A.

The electric field $\vec{E}(\theta, \phi)$ radiated from a horn at angles (θ, ϕ) is given by

$$\vec{E}(\theta, \phi) = E_\theta(\theta) \sin\phi \hat{a}_\theta + E_\phi(\theta) \cos\phi \hat{a}_\phi \tag{1}$$

where $E_\theta(\theta)$ and $E_\phi(\theta)$ are the E- and H-plane patterns (amplitude and phase). The $E_\theta(\theta)$ and $E_\phi(\theta)$ can be computed theoretically or experimentally measured. The E-field in the dichroic plate analysis is represented by the TE and TM polarizations:

$$\vec{E}(\theta', \phi') = A_{TE} \hat{a}_{TE} + A_{TM} \hat{a}_{TM} \tag{2}$$

where θ' and ϕ' are the angles of incidence. To integrate the horn pattern with the dichroic plate analysis, coordinate transformations between the horn coordinates $(\hat{a}_r\ \hat{a}_\theta\ \hat{a}_\phi)$ for spherical coordinates or $(\hat{a}_x\ \hat{a}_y\ \hat{a}_z)$ for Cartesian coordinates and the dichroic plate coordinates $(\hat{a}_{r'}\ \hat{a}_{\theta'}\ \hat{a}_{\phi'})$ or $(\hat{a}_{x'}\ \hat{a}_{y'}\ \hat{a}_{z'})$ are required and are presented in Appendix B.

The incident E-field [Eq. (1)] can be rewritten in a matrix form as

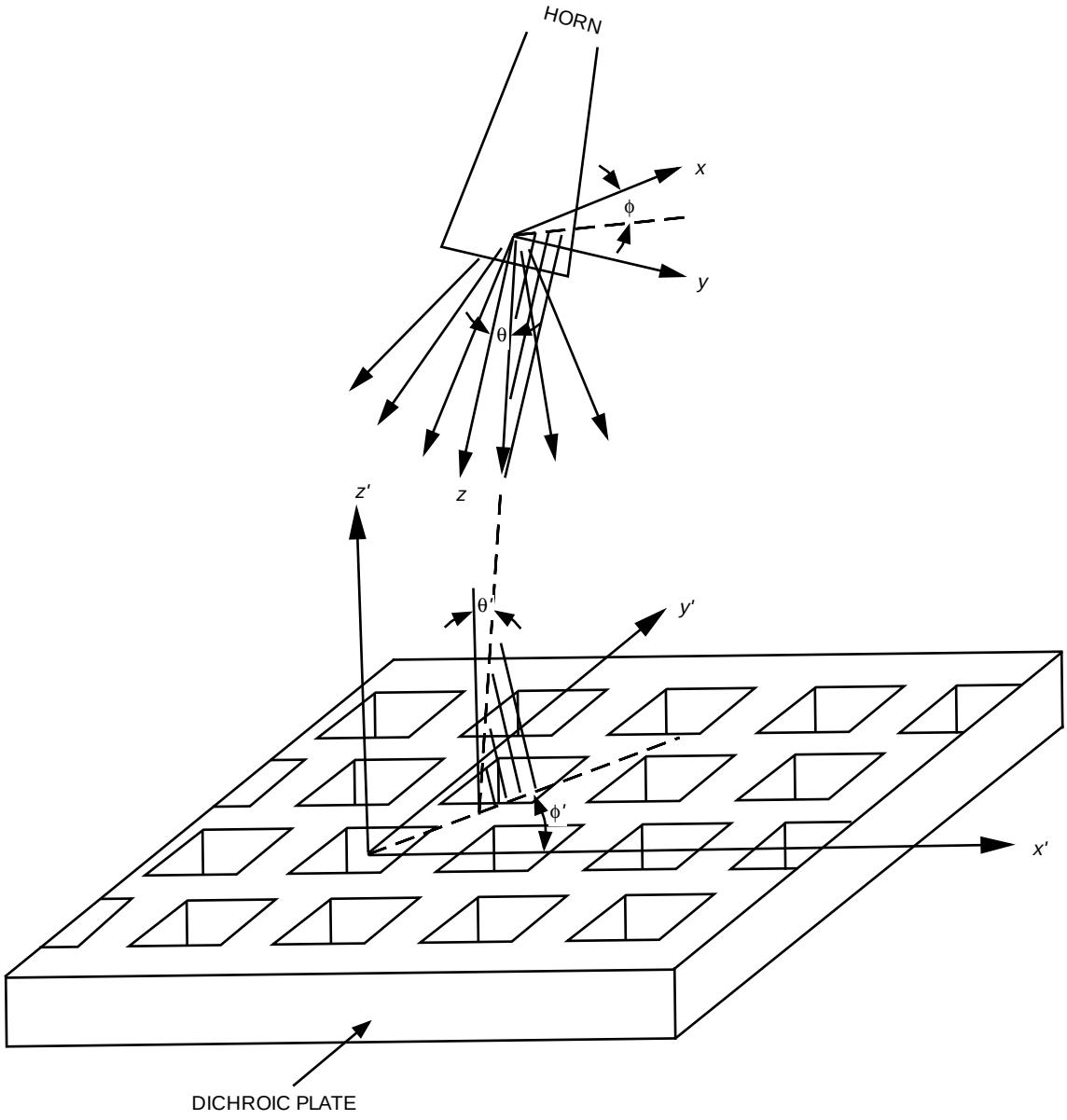

Fig. 2. The dichroic plate with horn pattern incidence.

$$\vec{E}^{inc} = \left[E^{inc}\right] \begin{bmatrix} \hat{a}_r \\ \hat{a}_\theta \\ \hat{a}_\phi \end{bmatrix} \tag{3}$$

Applying the coordinate transformations from the horn spherical coordinate to the dichroic plate Cartesian coordinate, the E-field becomes

$$\vec{E}^{inc} = \left[E^{inc}\right] [P] [R_{\alpha\beta\gamma}] \begin{bmatrix} \hat{a}_{x'} \\ \hat{a}_{y'} \\ \hat{a}_{z'} \end{bmatrix} \tag{4}$$

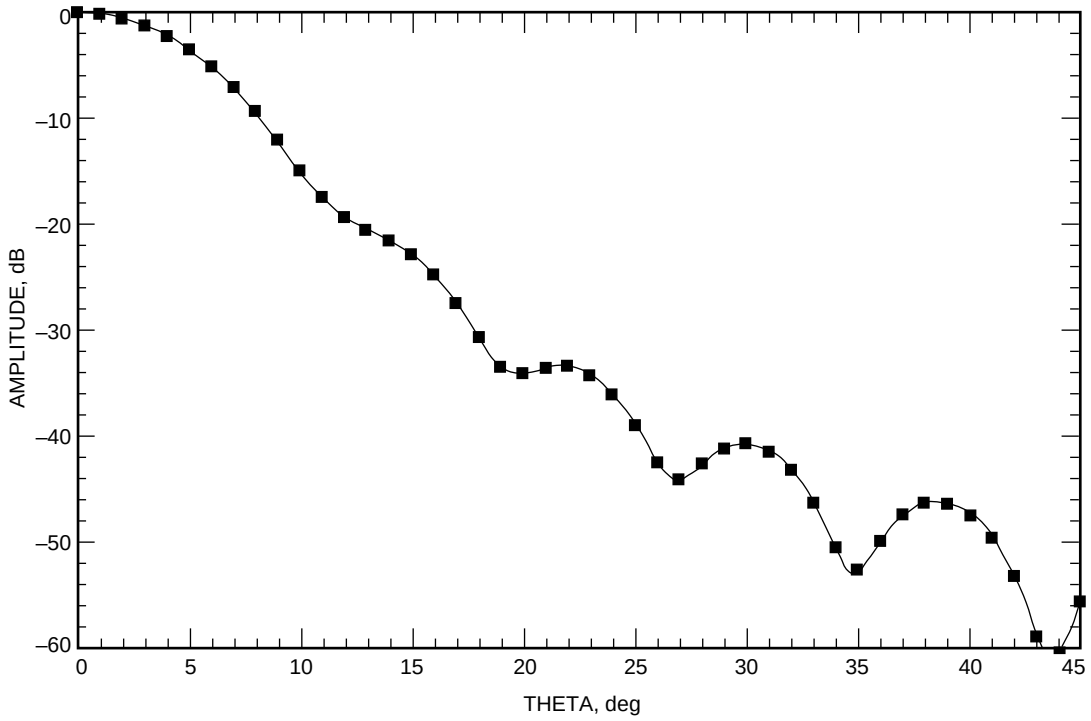

Fig. 3. The 26-dB horn pattern at 32.0 GHz sampled at 1-deg increments.

where $[P]$ is a 3×3 transformation matrix from spherical coordinates to Cartesian coordinates, and $[R_{\alpha\beta\gamma}]$ is a 3×3 Eulerian transformation matrix from the horn Cartesian coordinates to the dichroic plate Cartesian coordinates with Eulerian angles α, β, and γ (Appendix B) [2].

The E-field can also be represented by the TE and TM linear polarizations in the dichroic plate Cartesian coordinates:

$$\vec{E}^{inc} = [A_{TE} \quad A_{TM}] \begin{bmatrix} \hat{a}_{TE} \\ \hat{a}_{TM} \end{bmatrix} \tag{5}$$

where $\hat{a}_{TE}$ and $\hat{a}_{TM}$ are unit vectors of the TE and TM linear polarizations with angle of incidence θ', ϕ':

$$\hat{a}_{TE} = [-\sin\phi' \quad \cos\phi' \quad 0] \begin{bmatrix} \hat{a}_{x'} \\ \hat{a}_{y'} \\ \hat{a}_{z'} \end{bmatrix} \tag{6}$$

$$\hat{a}_{TM} = \frac{1}{\sqrt{1+\tan^2\theta'}} [-\cos\phi' \quad -\sin\phi' \quad \tan\theta'] \begin{bmatrix} \hat{a}_{x'} \\ \hat{a}_{y'} \\ \hat{a}_{z'} \end{bmatrix} \tag{7}$$

The A_{TE} and A_{TM} are the incident amplitude and phase on the TE and TM components of the field:

$$A_{TE} = \vec{E}^{inc} \cdot \hat{a}_{TE} \tag{8}$$

$$A_{TM} = \vec{E}^{inc} \cdot \hat{a}_{TM} \tag{9}$$

The incident E-field is changed from an E- and H-plane representation in the horn system to a TE and TM polarization representation in the dichroic plate system. Then the E-field is multiplied by the scattering matrices from the dichroic plate computer program:

$$\begin{bmatrix} B_{TE} \\ B_{TM} \end{bmatrix} = \begin{bmatrix} S^{21}_{TE,TE} & S^{21}_{TE,TM} \\ S^{21}_{TM,TE} & S^{21}_{TM,TM} \end{bmatrix} \begin{bmatrix} A_{TE} \\ A_{TM} \end{bmatrix} \tag{10}$$

$$\begin{bmatrix} C_{TE} \\ C_{TM} \end{bmatrix} = \begin{bmatrix} S^{11}_{TE,TE} & S^{11}_{TE,TM} \\ S^{11}_{TM,TE} & S^{11}_{TM,TM} \end{bmatrix} \begin{bmatrix} A_{TE} \\ A_{TM} \end{bmatrix} \tag{11}$$

where B_{TE} and B_{TM} are the transmitted amplitude and phase, and C_{TE} and C_{TM} are the reflected amplitude and phase for the TE and TM polarizations. The $[S^{21}]$ and $[S^{11}]$ are 2×2 scattering matrices containing transmission coefficients and reflection coefficients of the dichroic plate, respectively. Therefore, the transmitted and the reflected E-fields are

$$\vec{E}^{tran} = \begin{bmatrix} B_{TE} & B_{TM} \end{bmatrix} \begin{bmatrix} \hat{a}_{TE} \\ \hat{a}_{TM} \end{bmatrix} \tag{12}$$

$$\vec{E}^{refl} = \begin{bmatrix} C_{TE} & C_{TM} \end{bmatrix} \begin{bmatrix} \hat{a}_{TE} \\ \hat{a}_{TM} \end{bmatrix} \tag{13}$$

Reverse coordinate transformations are applied to the transmitted and reflected E-field in the TE and TM mode representations to obtain the E-plane and H-plane representations. By summing the E-fields of the plane waves at each point of the horn pattern in the transmitted and reflected direction, the reflected and transmitted patterns through the dichroic plate are computed. The same analysis technique can also be applied for circularly polarized incidence. The procedure is discussed in detail in Appendix B.

III. Reflected Horn Patterns and Noise Temperature Prediction

The horn pattern analysis was tested using an X-/Ka-/KABLE (Ka-Band Link Experiment)-band dichroic plate that reflects X-band (8.4 to 8.6 GHz) and passes Ka-band [3]. The design priorities for this plate were (1) Ka-band downlink of 31.8 to 32.4 GHz, (2) Ka-band uplink of 34.2 to 34.7 GHz, and (3) KABLE frequencies of 33.6 to 33.7 GHz. The design assumed plane-wave incidence at an angle of $\theta' = 30$ deg and $\phi' = 0$ deg. The Ka-band horn is a 26-dB corrugated horn. Figure 4 shows the Ka-band horn pattern at 34.5 GHz. The x- and y-axes on the plot represent ϕ' and θ', the angles of incidence on the plate. The curves are centered about $\phi' = 0$ deg and $\theta' = 30$ deg, where the central ray from the horn strikes the plate. The curves correspond to the $\theta = 0$-, 5-, 10-, 15-, 20-, and 25-deg contours of the horn pattern, which have intensities of 1.0, 0.419, 0.0345, 0.0045, 0.0005, and 0.00005, respectively, at 34.5 GHz.

Each plane wave strikes the plate at a different angle, and the transmission coefficients decrease as the angle of incidence gets farther from the design angle. The transmission coefficient of the dichroic plate is multiplied by the corresponding intensity of the horn pattern (Fig. 5). Also included in the figure is a grating lobe curve for 34.5 GHz. Grating lobes are generated when the angle of incidence is equal to or greater than the grating lobe angles. The transmitted energy drops substantially when the angle of incidence is above the grating lobe curve.

The X-/Ka-/KABLE-band dichroic plate/Ka-band 26-dB horn combination was measured in the chamber at antenna range. The horn patterns were measured at $\phi = 0$ and 90 deg for the two orthogonal linear polarizations at 32.0 and 33.7 GHz. The calculated and measured reflected radiation

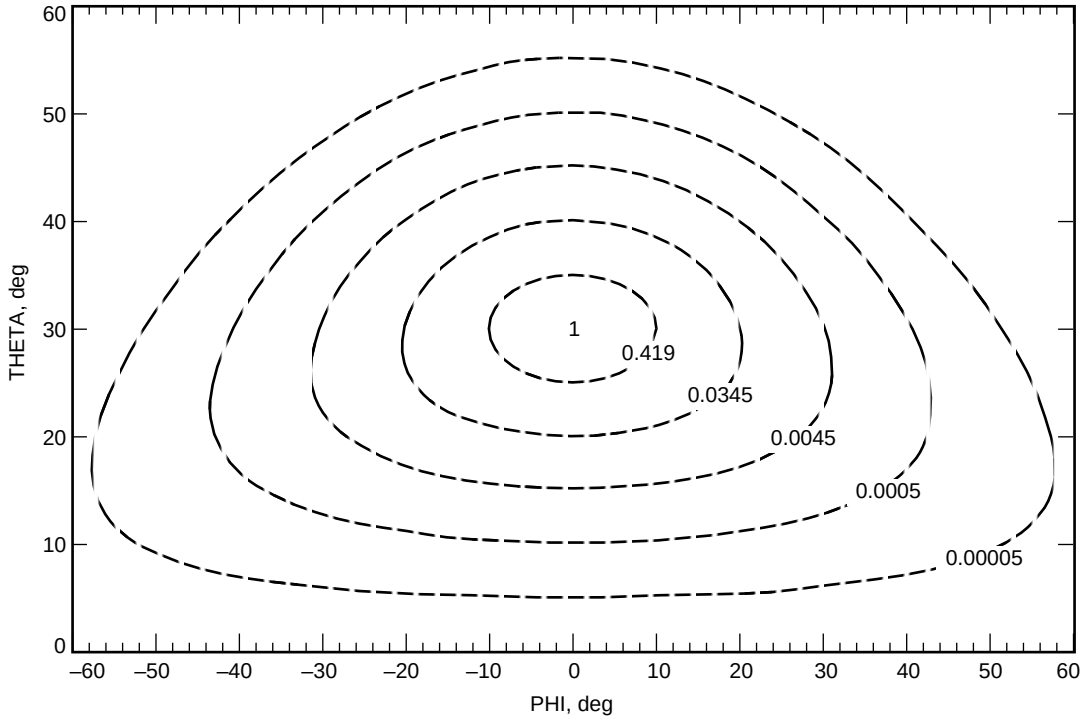

Fig. 4. Incident horn pattern at 34.5 GHz in the dichroic plate coordinates. The values shown are intensities.

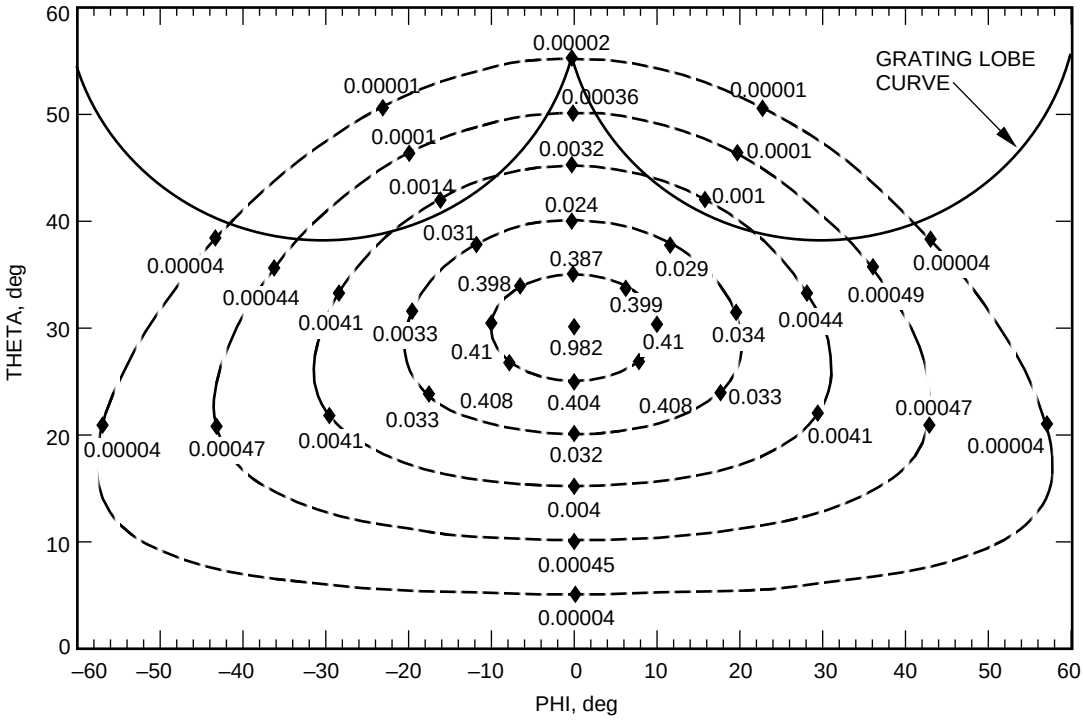

Fig. 5. Transmitted power through the dichroic plate with horn pattern incidence at 34.5 GHz. The values shown are intensities.

patterns are in good agreement (Figs. 6 through 13). The transmitted patterns were also calculated (Figs. 14 through 17).

The noise temperature was calculated for a pattern sampled at $\Delta\theta = 1$ deg up to 30 deg and for 32 ϕ-plane cuts. The noise temperature (NT) is the percentage of power lost multiplied by 300 K, which is the background temperature in the pedestal room at DSS 13:

$$NT = (1 - P^{tran})\ 300\ \text{K} \tag{14}$$

where P^{tran} is the total transmitted power. The horn pattern model predicts an extra 0.74 K at 32.0 GHz over the plane-wave model (originally 1.34 K) and an extra 1.72 K at 33.7 GHz over the plane wave model (originally 7.57 K) (Table 1). The measured noise temperature is 10.5 K at the KABLE frequency band. The noise temperature at 33.7 GHz is higher than that at 32.0 GHz because the X-/Ka-/Kable-band dichroic plate was optimized for the Ka-band downlink. The loss at 34.5 GHz (uplink) increases from 0.087 to 0.121 dB. The loss increment calculated in dB at 34.5 GHz is even higher than that at 33.7 GHz, due to grating lobes at this frequency. The noise temperature includes the reflection loss, conductivity loss, and grating lobe loss, if any. The loss due to dichroic plate surface roughness is not included.

IV. Conclusion

The analysis of a dichroic plate including horn pattern incidence was shown to be a better model for a real system than the plane-wave model. The discrepancy between the calculated and measured noise temperature is reduced. The theoretical and experimental reflected horn patterns show good agreement. The analysis for the beam waveguide antenna system can now include the effect of the dichroic plate on the transmitted radiation pattern. The success of this technique leads one to believe that it is feasible to modify the local characteristic of the dichroic plate on a point-by-point basis to improve performance.

Table 1. Noise temperature[a] contribution of the X-/Ka-/KABLE-band dichroic plate at the DSS-13 beam waveguide antenna.

Method	Frequency, GHz		
	32	33.7	34.5
Plane wave analysis, K	1.34	7.57	— (0.087 dB)
Horn pattern analysis, K	2.08	9.29	— (0.121 dB)
Measurement, K	—[b]	10.5[c]	—[d]

[a] The noise temperature calculated includes reflection loss and conductivity loss. Surface roughness is not included.
[b] To be determined.
[c] The noise temperature was measured in the frequency range of 33.65 to 33.75 GHz.
[d] Not applicable.

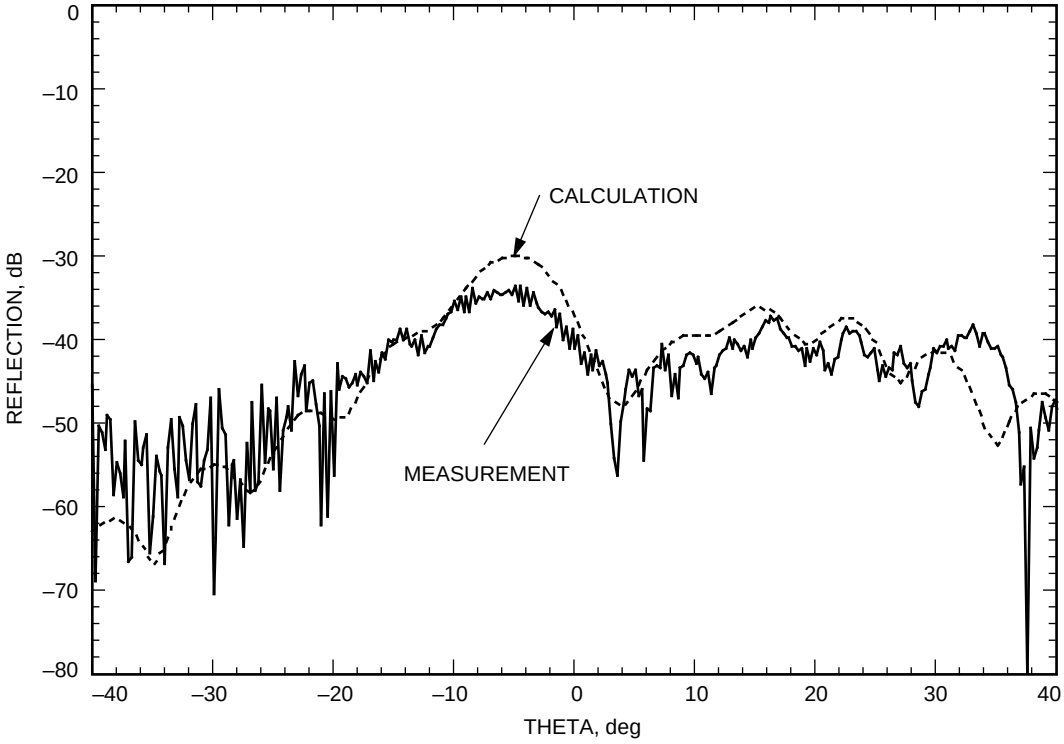

Fig. 6. Measured and calculated E_ϕ at ϕ = 0-deg cut at 32.0 GHz for linear polarization.

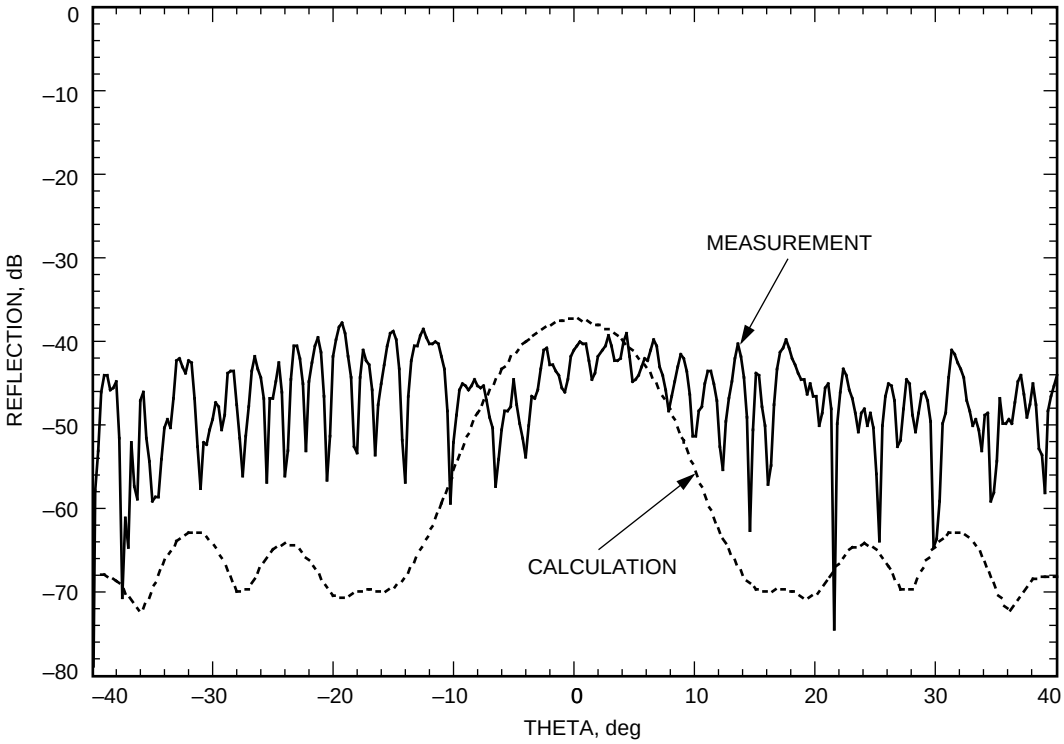

Fig. 7. Measured and calculated E_θ at ϕ = 90-deg cut at 32.0 GHz for linear polarization.

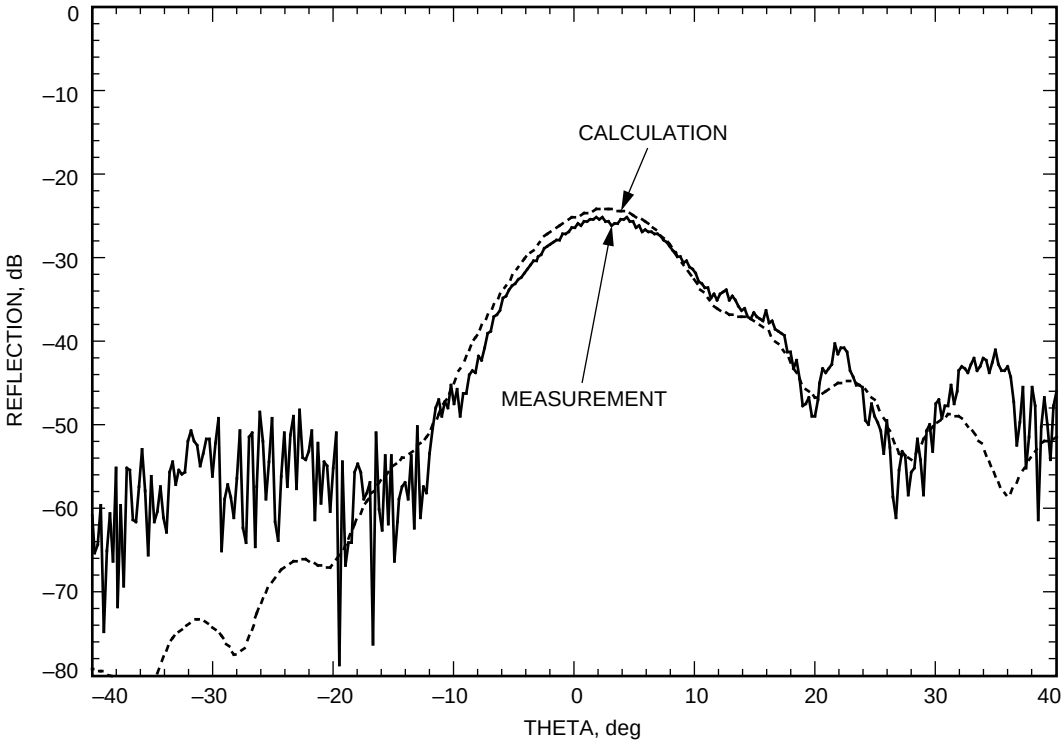

Fig. 8. Measured and calculated E_θ at ϕ = 0-deg at 32.0 GHz for orthogonal linear polarization.

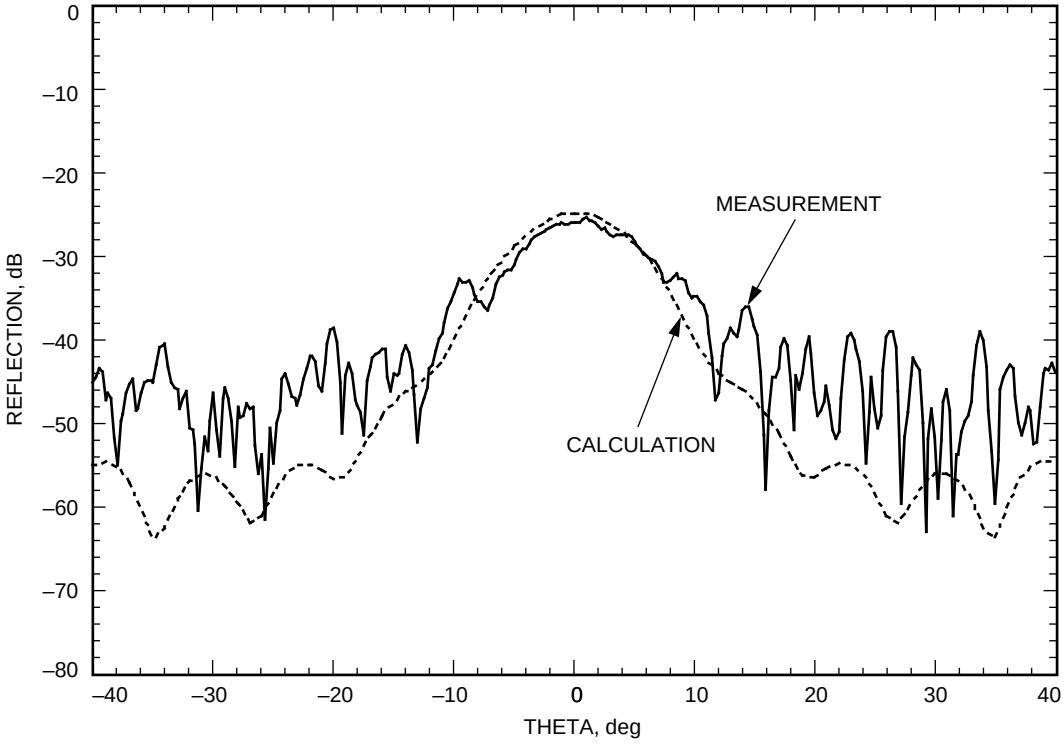

Fig. 9. Measured and calculated E_ϕ at ϕ = 90-deg at 32.0 GHz for orthogonal linear polarization.

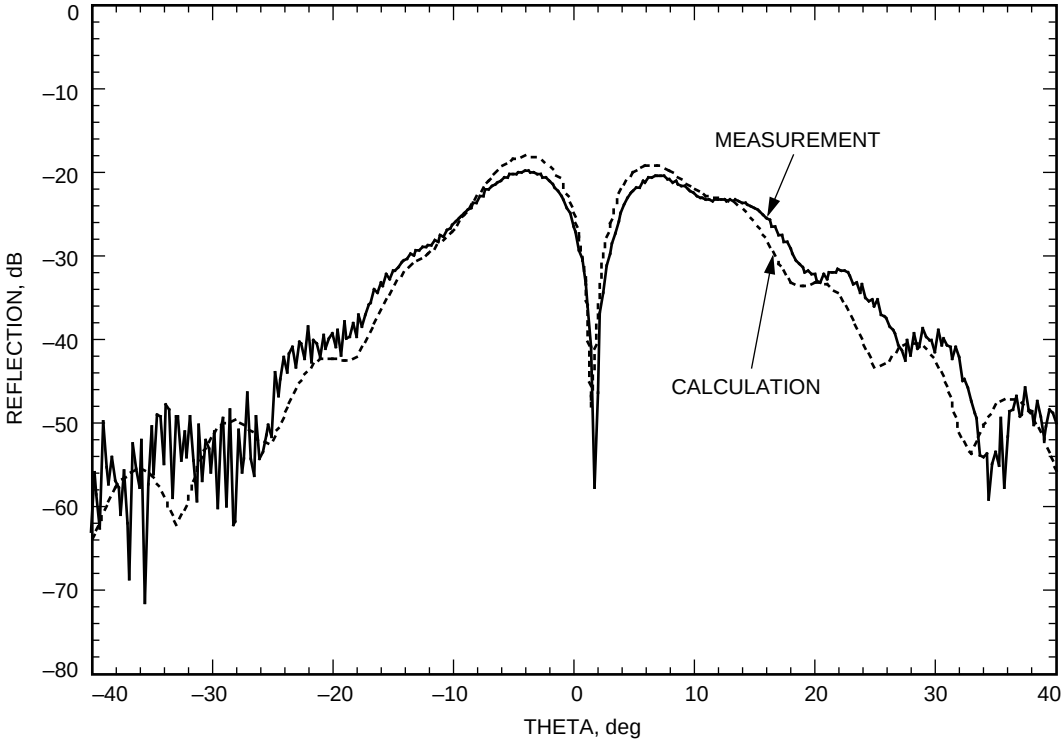

Fig. 10. Measured and calculated E_ϕ at ϕ = 0 deg at 33.7 GHz for linear polarization.

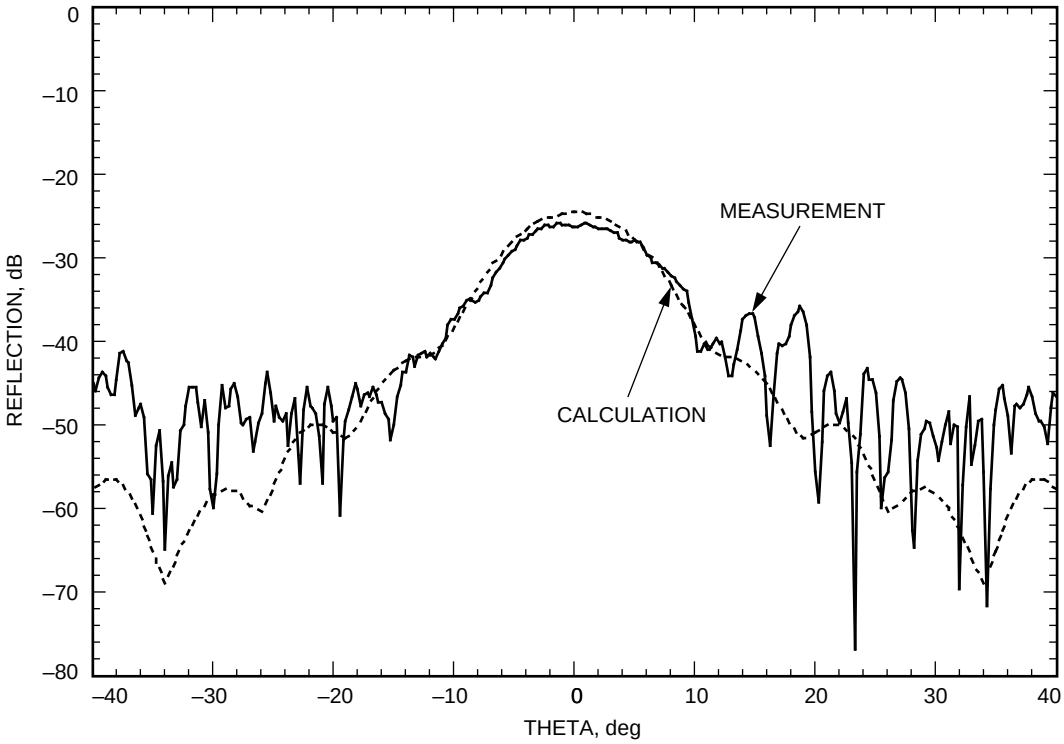

Fig. 11. Measured and calculated E_θ at ϕ = 90 deg at 33.7 GHz for linear polarization.

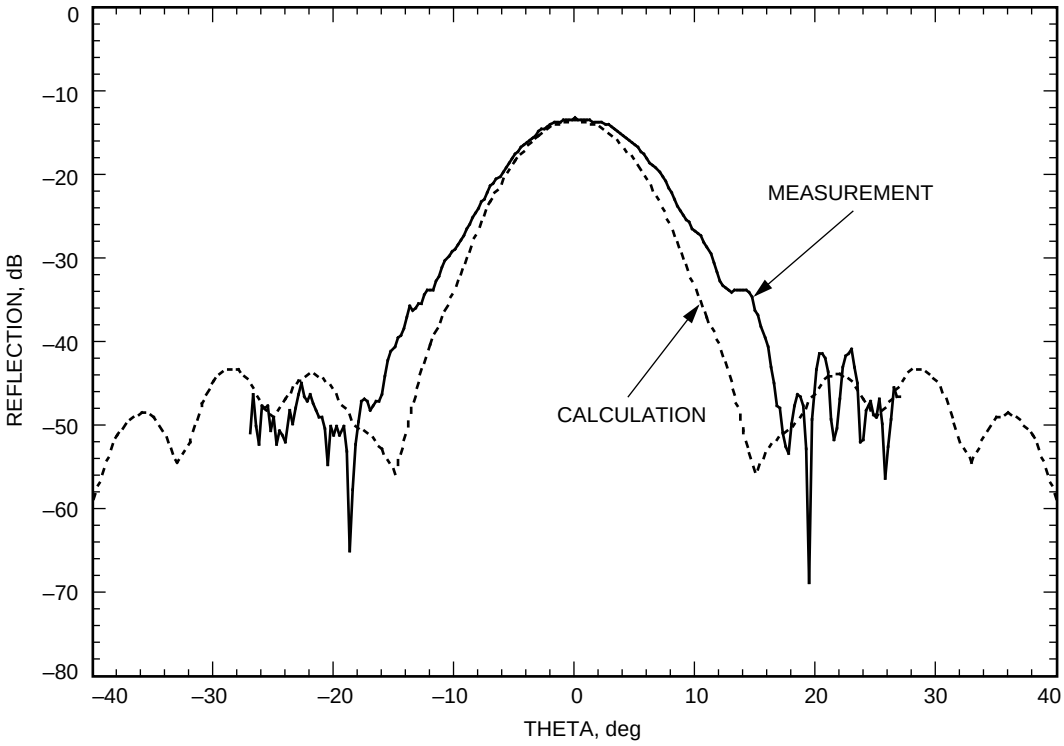

Fig. 12. Measured and calculated E_θ at ϕ = 0 deg at 33.7 GHz for orthogonal linear polarization.

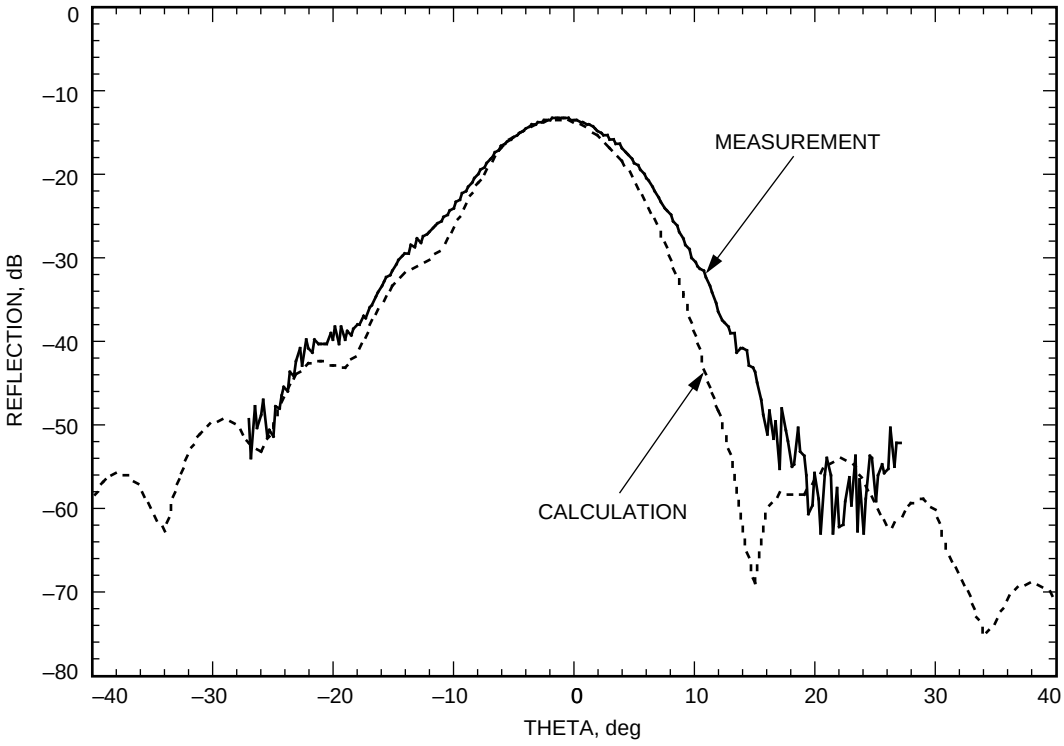

Fig. 13. Measured and calculated E_ϕ at ϕ = 90 deg at 33.7 GHz for orthogonal linear polarization.

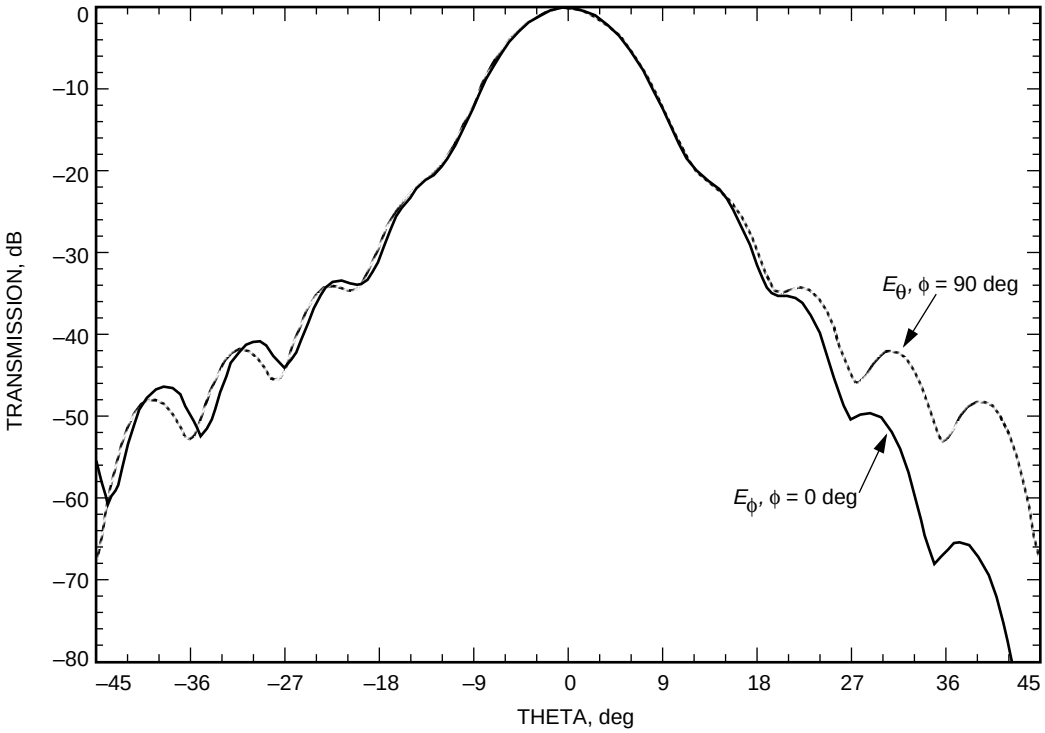

Fig. 14. Calculated transmitted pattern for the X-/Ka-/KABLE-band dichroic plate at 32.0 GHz for linear polarization.

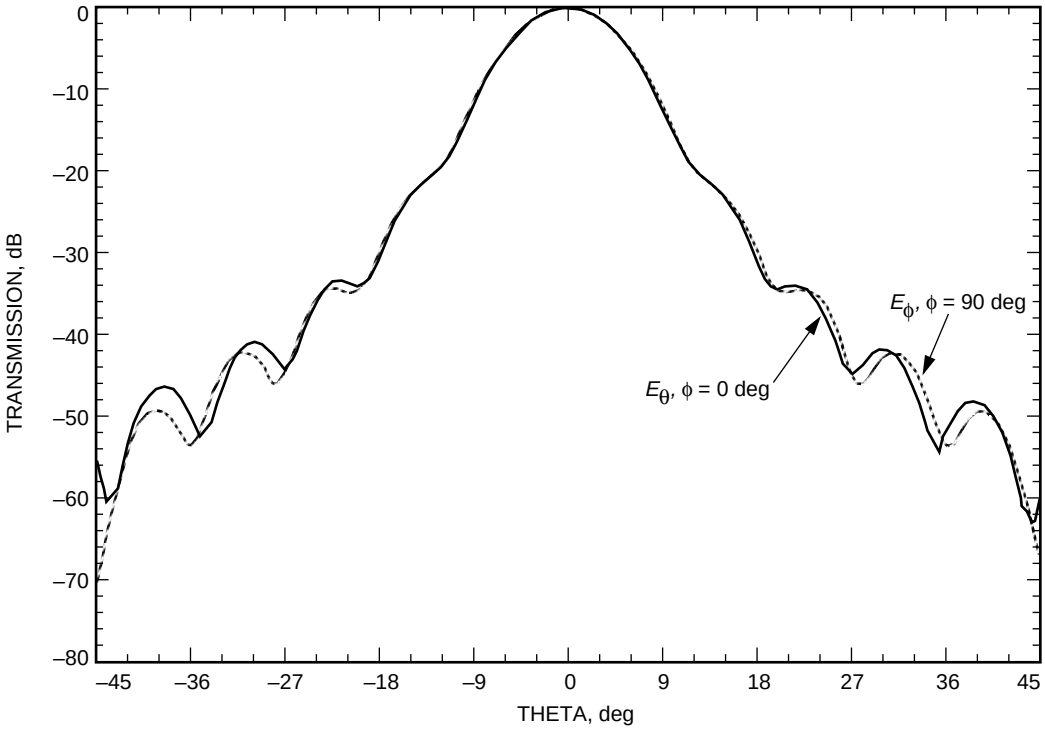

Fig. 15. Calculated transmitted pattern for the X-/Ka-/KABLE-band dichroic plate at 32.0 GHz for orthogonal linear polarization.

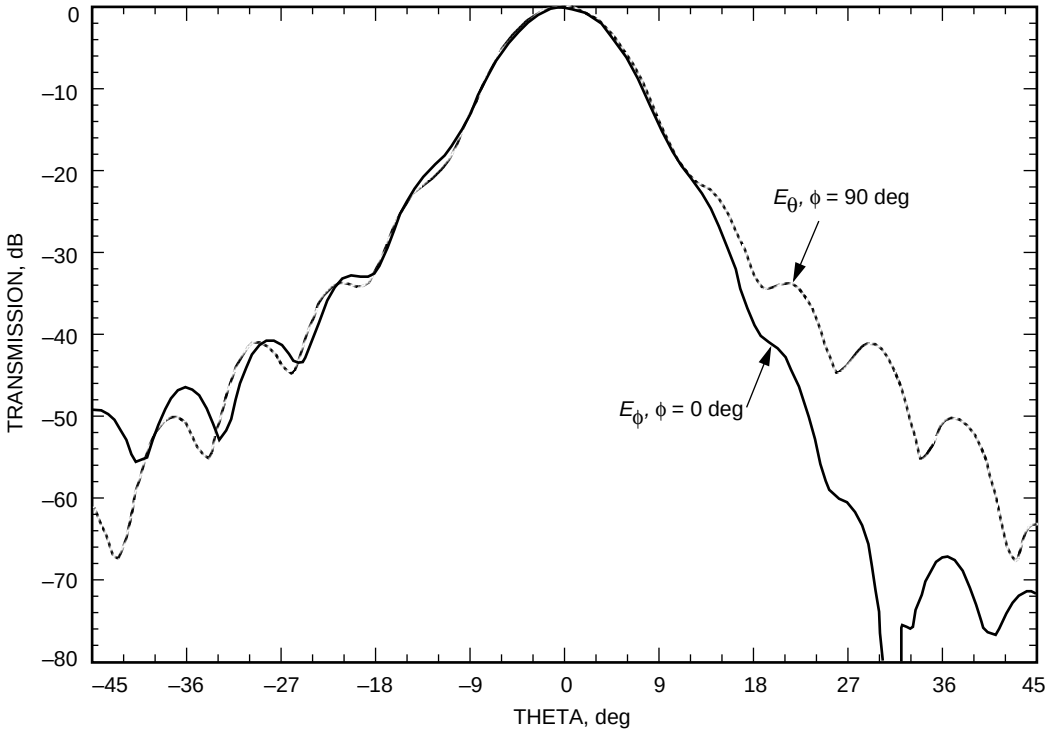

Fig. 16. Calculated transmitted pattern for the X-/Ka-/KABLE-band dichroic plate at 33.7 GHz for linear polarization.

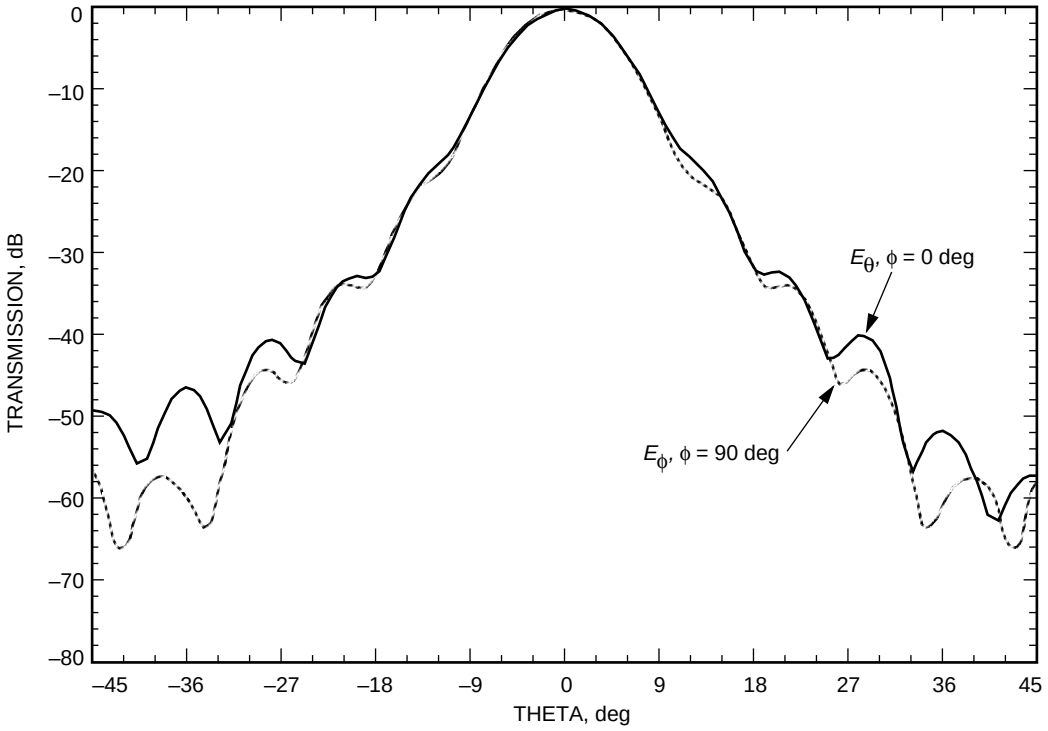

Fig. 17. Calculated transmitted pattern for the X-/Ka-/KABLE-band dichroic plate at 33.7 GHz for orthogonal linear polarization.

Acknowledgments

The author would like to acknowledge D. J. Hoppe for the technical discussions and J. Withington for the experimental patterns. The Cray supercomputer used in this investigation was provided by funding from the NASA Offices of Mission to Planet Earth, Aeronautics, and Space Science.

References

[1] J. C. Chen, "Analysis of a Thick Dichroic Plate with Rectangular Holes at Arbitrary Angles of Incidence," *The Telecommunications and Data Acquisition Progress Report 42-104, vol. October–December 1990*, Jet Propulsion Laboratory, Pasadena, California, pp. 9–16, February 15, 1991.

[2] J. B. Marion, *Classical Dynamics of Particles and Systems*, 2nd ed., West Philadelphia, Pennsylvania: Saunders College Publications, pp. 384–385.

[3] J. C. Chen, "X-/Ka-Band Dichroic Plate Design and Grating Lobe Study," *The Telecommunications and Data Acquisition Progress Report 42-105, vol. January–March 1991*, Jet Propulsion Laboratory, Pasadena, California, pp. 21–30, May 15, 1991.

Appendix A

Computation of Angles of Incidence on a Dichroic Plate for the Horn Radiation Pattern

A plane wave traveling in the direction (θ, ϕ) in the horn coordinate system will strike the dichroic plate at an incident angle (θ', ϕ') in the dichroic plate coordinate system.

Suppose the energy radiated from the horn is in the direction $\vec{r}$:

$$\vec{r} = [\,1 \quad 0 \quad 0\,] \begin{bmatrix} \hat{a}_r \\ \hat{a}_\theta \\ \hat{a}_\phi \end{bmatrix} \tag{A-1}$$

We may transform the spherical coordinate system to the Cartesian coordinate system using

$$\begin{bmatrix} \hat{a}_r \\ \hat{a}_\theta \\ \hat{a}_\phi \end{bmatrix} = [P] \begin{bmatrix} \hat{a}_x \\ \hat{a}_y \\ \hat{a}_z \end{bmatrix} \tag{A-2}$$

where $[P]$ is the following 3×3 matrix:

$$[P] = \begin{bmatrix} \sin\theta\cos\phi & \sin\theta\sin\phi & \cos\theta \\ \cos\theta\cos\phi & \cos\theta\sin\phi & -\sin\phi \\ -\sin\phi & \cos\phi & 0 \end{bmatrix} \tag{A-3}$$

Transforming the horn coordinate system ($x\ y\ z$) to the dichroic plate coordinate system ($x'\ y'\ z'$) using Eulerian angles α, β, and γ, we have

$$\begin{bmatrix} \hat{a}_x \\ \hat{a}_y \\ \hat{a}_z \end{bmatrix} = [R_{\alpha\beta\gamma}] \begin{bmatrix} \hat{a}_{x'} \\ \hat{a}_{y'} \\ \hat{a}_{z'} \end{bmatrix} \tag{A-4}$$

where $[R_{\alpha\beta\gamma}]$ is the following 3×3 matrix:

$$[R_{\alpha\beta\gamma}] = \begin{bmatrix} \cos\gamma\cos\alpha - \cos\beta\sin\alpha\sin\gamma & \cos\gamma\sin\alpha + \cos\beta\cos\alpha\sin\gamma & \sin\gamma\sin\beta \\ -\sin\gamma\cos\alpha - \cos\beta\sin\alpha\cos\gamma & -\sin\gamma\sin\alpha + \cos\beta\cos\alpha\cos\gamma & \cos\gamma\sin\beta \\ \sin\beta\sin\alpha & -\sin\beta\cos\alpha & \cos\beta \end{bmatrix} \tag{A-5}$$

Therefore,

$$\vec{r} = [\,1 \quad 0 \quad 0\,] \begin{bmatrix} \hat{a}_r \\ \hat{a}_\theta \\ \hat{a}_\phi \end{bmatrix} \tag{A-6}$$

$$= [\,1 \quad 0 \quad 0\,]\,[P] \begin{bmatrix} \hat{a}_x \\ \hat{a}_y \\ \hat{a}_z \end{bmatrix} \tag{A-7}$$

$$= [\,1 \quad 0 \quad 0\,]\,[P]\,[R_{\alpha\beta\gamma}] \begin{bmatrix} \hat{a}_{x'} \\ \hat{a}_{y'} \\ \hat{a}_{z'} \end{bmatrix} \tag{A-8}$$

$$= [\,x' \quad y' \quad z'\,] \begin{bmatrix} \hat{a}_{x'} \\ \hat{a}_{y'} \\ \hat{a}_{z'} \end{bmatrix} \tag{A-9}$$

where

$$x'^2 + y'^2 + z'^2 = 1 \tag{A-10}$$

The $\vec{r}$ vector can also be written in the dichroic plate system:

$$\vec{r} = [\,1 \quad 0 \quad 0\,] \begin{bmatrix} \hat{a}_{r'} \\ \hat{a}_{\theta'} \\ \hat{a}_{\phi'} \end{bmatrix} \tag{A-11}$$

$$= [\,1 \quad 0 \quad 0\,]\,[P_{\theta'\phi'}] \begin{bmatrix} \hat{a}_{x'} \\ \hat{a}_{y'} \\ \hat{a}_{z'} \end{bmatrix} \tag{A-12}$$

$$= \left[\sin\theta'\sin\phi' \quad \sin\theta'\cos\phi' \quad \cos\theta'\right] \begin{bmatrix} \hat{a}_{x'} \\ \hat{a}_{y'} \\ \hat{a}_{z'} \end{bmatrix} \tag{A-13}$$

Comparing Eqs. (A-8), (A-9), and (A-13), we have

$$\left[\sin\theta'\sin\phi' \quad \sin\theta'\cos\phi' \quad \cos\theta'\right] = \left[1 \quad 0 \quad 0\right][P][R_{\alpha\beta\gamma}] = \left[x' \quad y' \quad z'\right] \tag{A-14}$$

The wave is traveling in the $-z'$ direction; therefore, the incident angle is the angle between the normal of the dichroic plate, $\vec{z}\,' = (0\ 0\ 1)$ and $-\vec{r} = (-x\ -y\ -z)$. The incident angles on the dichroic plate (θ', ϕ') are then

$$\theta' = \arctan\left(-\frac{\sqrt{x'^2 + y'^2}}{z'}\right) \tag{A-15}$$

$$\phi' = \arctan\left(\frac{y'}{x'}\right) \tag{A-16}$$

Appendix B

Computation of Reflected and Transmitted Electric Fields for a Dichroic Plate

I. The *E*-Field Represented by the *E*- and *H*-Plane Polarizations

The electric field $\vec{E}(\theta, \phi)$ radiated by the horn is traveling in the r direction with angles (θ, ϕ):

$$\vec{E}(\theta, \phi) = E_\theta(\theta)\sin\phi\hat{a}_\theta + E_\phi(\theta)\cos\phi\hat{a}_\phi \tag{B-1}$$

where $E_\theta(\theta)$ and $E\phi(\theta)$ are the E- and H-plane patterns (amplitude and phase). The incident electrical field can be rewritten in matrix form:

$$\vec{E}^{inc}(\theta, \phi) = \left[0 \quad E_\theta^{inc}(\theta)\sin\phi \quad E_\phi^{inc}(\theta)\cos\phi\right] \begin{bmatrix} \hat{a}_r \\ \hat{a}_\theta \\ \hat{a}_\phi \end{bmatrix} = [E^{inc}] \begin{bmatrix} \hat{a}_r \\ \hat{a}_\theta \\ \hat{a}_\phi \end{bmatrix} \tag{B-2}$$

where $[E^{inc}]$ is a 1×3 matrix.

The spherical coordinates $(r\ \theta\ \varphi)$ are transformed to Cartesian coordinates $(x\ y\ z)$ in the horn coordinate system using

$$\begin{bmatrix} \hat{a}_r \\ \hat{a}_\theta \\ \hat{a}_\phi \end{bmatrix} = [P] \begin{bmatrix} \hat{a}_x \\ \hat{a}_y \\ \hat{a}_z \end{bmatrix} \tag{B-3}$$

where [P] is a 3 x 3 matrix given in Eq. (A-3). The E-field can be expressed as

$$\vec{E}^{inc} = \left[E^{inc}\right][P] \begin{bmatrix} \hat{a}_x \\ \hat{a}_y \\ \hat{a}_z \end{bmatrix} \tag{B-4}$$

The transformation from the dichroic plate coordinate system (x' y' z') to the horn coordinate system (x y z) using Eulerian angles α, β, and γ is shown below:

$$\begin{bmatrix} \hat{a}_x \\ \hat{a}_y \\ \hat{a}_z \end{bmatrix} = [R_{\alpha\beta\gamma}] \begin{bmatrix} \hat{a}_{x'} \\ \hat{a}_{y'} \\ \hat{a}_{z'} \end{bmatrix} \tag{B-5}$$

where $[R_{\alpha\beta\gamma}]$ is a 3×3 matrix given in Eq. (A-5). Therefore, the E-field is

$$\vec{E}^{inc} = \left[E^{inc}\right] \begin{bmatrix} \hat{a}_r \\ \hat{a}_\theta \\ \hat{a}_\phi \end{bmatrix} \tag{B-6}$$

$$= \left[E^{inc}\right][P] \begin{bmatrix} \hat{a}_x \\ \hat{a}_y \\ \hat{a}_z \end{bmatrix} \tag{B-7}$$

$$= \left[E^{inc}\right][P][R_{\alpha\beta\gamma}] \begin{bmatrix} \hat{a}_{x'} \\ \hat{a}_{y'} \\ \hat{a}_{z'} \end{bmatrix} \tag{B-8}$$

II. The *E*-Field Represented by the *TE* and *TM* Modes

The E-field can also be represented by TE and TM components in the dichroic plate coordinates (x' y' z'):

$$\vec{E}^{inc} = [A_{TE} \quad A_{TM}] \begin{bmatrix} \hat{a}_{TE} \\ \hat{a}_{TM} \end{bmatrix} \tag{B-9}$$

where $\hat{a}_{TE}$ and $\hat{a}_{TM}$ are unit vectors of the TE and TM linear polarizations at angles of incidence θ', ϕ':

$$\hat{a}_{TE} = [-\sin\phi' \quad \cos\phi' \quad 0] \begin{bmatrix} \hat{a}_{x'} \\ \hat{a}_{y'} \\ \hat{a}_{z'} \end{bmatrix} = [\Psi_{TE}] \begin{bmatrix} \hat{a}_{x'} \\ \hat{a}_{y'} \\ \hat{a}_{z'} \end{bmatrix} \tag{B-10}$$

$$\hat{a}_{TM} = \frac{1}{\sqrt{1+\tan^2\theta'}}\left[-\cos\phi' \quad -\sin\phi' \quad \tan\theta'\right]\begin{bmatrix}\hat{a}_{x'}\\ \hat{a}_{y'}\\ \hat{a}_{z'}\end{bmatrix} = [\Psi_{TM}]\begin{bmatrix}\hat{a}_{x'}\\ \hat{a}_{y'}\\ \hat{a}_{z'}\end{bmatrix} \tag{B-11}$$

Note that

$$|\hat{a}_{TE}| = 1 \tag{B-12}$$

$$|\hat{a}_{TM}| = 1 \tag{B-13}$$

$$\hat{a}_{TE}\cdot\hat{a}_{TM} = 0 \tag{B-14}$$

$$\hat{a}_{TE}\cdot\hat{a}_{r'} = 0 \tag{B-15}$$

$$\hat{a}_{TM}\cdot\hat{a}_{r'} = 0 \tag{B-16}$$

The A_{TE} and A_{TM} are the incident amplitude and phase in the directions of the TE and TM polarizations, respectively.

$$A_{TE} = \vec{E}^{inc}\cdot\hat{a}_{TE} \tag{B-17}$$

$$A_{TM} = \vec{E}^{inc}\cdot\hat{a}_{TM} \tag{B-18}$$

By Eqs. (B-8), (B-10), and (B-11), we have

$$A_{TE} = [E^{inc}][P]\,[R_{\alpha\beta\gamma}]\,[\Psi_{TE}]^T \tag{B-19}$$

$$A_{TM} = [E^{inc}][P]\,[R_{\alpha\beta\gamma}]\,[\Psi_{TM}]^T \tag{B-20}$$

where $[\Psi_{TE}]^T$ and $[\Psi_{TM}]^T$ are the transpose matrices of $[\Psi_{TE}]$ and $[\Psi_{TM}]$, respectively.

III. The Dichroic Plate Scattering Matrix

After the wave strikes the dichroic plate, the transmitted and reflected E-fields are given by

$$\vec{E}^{tran} = [\,B_{TE} \quad B_{TM}\,]\begin{bmatrix}\hat{a}_{TE}\\ \hat{a}_{TM}\end{bmatrix}$$

$$\vec{E}^{refl} = [\,C_{TE} \quad C_{TM}\,]\begin{bmatrix}\hat{a}_{TE}\\ \hat{a}_{TM}\end{bmatrix}$$

where B_{TE} and B_{TM} are the TE and TM components for the transmitted E-field, and C_{TE} and C_{TM} are the TE and TM components for the reflected E-field and are given by

$$\begin{bmatrix} B_{TE} \\ B_{TM} \end{bmatrix} = \begin{bmatrix} S^{21}_{TE,TE} & S^{21}_{TE,TM} \\ S^{21}_{TM,TE} & S^{21}_{TM,TM} \end{bmatrix} \begin{bmatrix} A_{TE} \\ A_{TM} \end{bmatrix} \tag{B-21}$$

$$\begin{bmatrix} C_{TE} \\ C_{TM} \end{bmatrix} = \begin{bmatrix} S^{11}_{TE,TE} & S^{11}_{TE,TM} \\ S^{11}_{TM,TE} & S^{11}_{TM,TM} \end{bmatrix} \begin{bmatrix} A_{TE} \\ A_{TM} \end{bmatrix} \tag{B-22}$$

where $[S^{21}]$ and $[S^{11}]$ are 2×2 dichroic plate scattering matrices containing transmission coefficients and reflection coefficients, respectively. The scattering matrix of the dichroic plate is calculated by a computer program using a plane-wave incidence model.

IV. Transforming Back to the *E*- and *H*-Plane Patterns

Applying the same coordinate transformation to $[E^{tran}]$, we have

$$\vec{E}^{tran} = \left[E^{tran}\right][P]\left[R_{\alpha\beta\gamma}\right] \begin{bmatrix} \hat{a}_{x'} \\ \hat{a}_{y'} \\ \hat{a}_{z'} \end{bmatrix} = \begin{bmatrix} B_{TE} & B_{TM} \end{bmatrix} \begin{bmatrix} \hat{a}_{TE} \\ \hat{a}_{TM} \end{bmatrix} \tag{B-23}$$

or

$$\left[E^{tran}\right][P]\left[R_{\alpha\beta\gamma}\right] = \begin{bmatrix} -B_{TE}\sin\phi' - B_{TM}\frac{\cos\phi'}{\sqrt{1+\tan^2\theta'}} & B_{TE}\cos\phi' - B_{TM}\frac{\sin\phi'}{\sqrt{1+\tan^2\theta'}} & B_{TM}\frac{\tan\theta'}{\sqrt{1+\tan^2\theta'}} \end{bmatrix} \tag{B-24}$$

$$\left[E^{tran}\right] = \begin{bmatrix} -B_{TE}\sin\phi' - B_{TM}\frac{\cos\phi'}{\sqrt{1+\tan^2\theta'}} & B_{TE}\cos\phi' - B_{TM}\frac{\sin\phi'}{\sqrt{1+\tan^2\theta'}} & B_{TM}\frac{\tan\theta'}{\sqrt{1+\tan^2\theta'}} \end{bmatrix} \left[R_{\alpha\beta\gamma}\right]^T [P]^T \tag{B-25}$$

Likewise, the reflected pattern is given by

$$\left[E^{refl}\right] = \begin{bmatrix} -C_{TE}\sin\phi' - C_{TM}\frac{\cos\phi'}{\sqrt{1+\tan^2\theta'}} & C_{TE}\cos\phi' - C_{TM}\frac{\sin\phi'}{\sqrt{1+\tan^2\theta'}} & C_{TM}\frac{\tan\theta'}{\sqrt{1+\tan^2\theta'}} \end{bmatrix} \left[R_{\alpha\beta\gamma}\right]^T [P]^T \tag{B-26}$$

V. Orthogonal Linear Polarization and Circular Polarization

The same method can apply to the orthogonal linear polarization and the circular polarization as well.

For the other linear polarization, the E-field is

$$\vec{E}(\theta,\phi) = E_\theta(\theta)\cos\phi\hat{a}_\theta + E_\phi(\theta)\sin\phi\hat{a}_\phi \tag{B-27}$$

and for circular polarization,

$$\vec{E}(\theta,\phi) = \frac{1}{\sqrt{2}}E_\theta(\theta)(\cos\phi + j\sin\phi)\hat{a}_\theta + \frac{1}{\sqrt{2}}E_\phi(\theta)(\sin\phi + j\cos\phi)\hat{a}_\phi \tag{B-28}$$